Educational Administration: Theory and Practice
2024, 30(10), 881-897
ISSN: 2148-2403
https://kuey.net/

Research Article

Black Widow-Based Optimal SVM and Fuzzy Segmentation for Classifying Skin Diseases

Dr. R. Sivakumar[1*], Dr. A. Manikandan[2], Dr. S. Mohan[3], Name. G. Kadirvel[4]

[1]Assistant Professor, Department of CSE(IoT), Paavai Engineering College, Namakkal (Dt), Tamilnadu, India,
Email: sivakumarranganathanpec@paavai.edu.in
[2]Professor, Department of CSE, Paavai Engineering College, Namakka (Dt) Tamilnadu, India,
Email: manikandanarumugampec@paavai.edu.in
[3]Assistant Professor, Department of ECE, Mahendra Engineering College, Namakkal, Email: smohhanbe@gmail.com
[4]Assistant professor, Department of ECE, The kavery engineering college, Email: infokadhir@gmail.com

Citation: Dr. R.Sivakumar, et.al (2024). Black Widow-Based Optimal SVM and Fuzzy Segmentation for Classifying Skin Diseases, *Educational Administration: Theory and Practice*, 30(10) 881-897
Doi: 10.53555/kuey.v30i10.10408

ARTICLE INFO

ABSTRACT

The primary human organ and external barrier is the skin, which is composed of seven layers. Skin cancer is the fourth most common cause of non-fatal disease risk, according to the World Health Organisation (WHO). Classifying skin diseases is a difficult problem in the medical field because of overfitting, erroneous results, higher computational costs, and other factors. We introduced a brand-new method for classifying skin diseases called support vector machine–based black widow optimisation, or SVM-BWO. Images of five distinct skin diseases—psoriasis, paederus, herpes, melanoma, and benign—as well as healthy ones are selected for this project. The original input images' noise is eliminated through the preprocessing step. The skin lesion region is then segmented using the new fuzzy set segmentation algorithm. The colour, gray-level co-occurrence matrix texture, and shape features are then taken out for additional processing. The SVM-BWO algorithm is used to classify skin diseases. Since MATLAB-2018a is used for implementation tasks, ISIC-2018 datasets were used to gather the dataset images. Various types of performance analyses are conducted experimentally using cutting-edge methods. In any case, the suggested methodology performs better than alternative approaches, with a 92% classification accuracy.

1 Introduction:

The biggest organ in the human body, the skin, is a common site for bacterial, viral, and inflammatory infections that can result in a number of skin conditions and other health issues. Vitiligo, wrinkles, psoriasis, wounds, photoaging, melanoma, morphea, alopecia, atopic dermatitis, and acne are examples of common skin conditions. The most deadly kind of skin cancer is malignant melanoma, and patient survival depends on early detection. Among the most prevalent forms of malignant epidermal lesions is basal cell carcinoma (BCC). For the diagnosis of pigmented skin lesions, radiologists and physicians employ gold standard imaging methods such as dermatoscopy or dermoscopy. For the treatment and early detection of skin diseases, sophisticated image processing techniques and computer-based diagnostic tools are helpful.

Identification and early treatment of skin cancer is a difficult problem that has been studied recently. Inflammatory skin conditions, psoriasis, fungal skin, scleroderma, varicella, candidiasis, cellulitis, and acne can all lead to serious death if left untreated. Because different skin lesions can have similar complex appearances, including color, texture, and shape, it can be difficult to distinguish between different skin diseases. The similarity between melanoma manifestation and dysplastic nevi is characterized by the melanocytic skin lesion. Over 1000 million people worldwide suffer from a variety of skin conditions. Primary and secondary stages are used to classify skin lesions. Primary skin lesions include the bulla, cyst, pustule, vesicle, nodule, discoloration, plaque, pimples, and spots. Phyma, umbilication, maceration, atrophy, induration, fissure, ulcer, scale, excoriation, erosion, and crust are also features of the second stage. Skin lesions have an impact on both distribution and configuration. Distribution provides information about the location of the lesion and how the lesions are grouped in accordance with the configuration.

The three main skin conditions—squamous cell disease (SC), melanoma, and seborrheic keratosis (SK)—are taken into consideration in the majority of current research.

Numerous researchers have developed various techniques for identifying skin conditions in the past few decades. The natural computing framework, region of interest (ROI), gray-level cooccurrence matrix (GLCM), fractal-based regional texture analysis (FRTA) feature extraction techniques, and various machine learning algorithms, including artificial neural networks (ANN), convolutional neural networks (CNN), generative adversarial networks (GANs) with support vector machines (SVM), naive Bayes (NB), K-nearest neighboring (kNN), and others, were also introduced. These techniques produced improved classification accuracy for skin disease identification, but they have a few drawbacks, including higher computational complexity in the dimensionality space, longer processing times, overfitting issues, noisy environments, inability to detect specific objects with changes in light intensity, sensitivity to noise that entirely depends on the region threshold for integration, high computational costs, user dependence, and the use of large feature vector dimensions.

We suggested a support vector machine–based black widow optimization (SVM-BWO) algorithm for efficient skin disease classification in order to get around this. The level set technique and spatial information from fuzzy c-means clustering are used in the proposed work to improve the clustering process. Images of five different types of skin diseases—psoriasis, paederus, herpes, melanoma, and benign—as well as healthy images are chosen for the classification of skin diseases. The skin lesion region is then segmented using the new fuzzy set segmentation algorithm. The color, GLCM texture, and shape features are then taken out for additional processing. Both the normal and abnormal skin disease classes are categorized using the SVM-BWO algorithm. The suggested approach outperforms current approaches like the radial basis function (RBF) and SVM, DCNN, DNN, and ANN in terms of accuracy, specificity, sensitivity, precision, and recall metrics. Healthy, psoriasis, paederus, herpes, melanoma, and benign provide 100%, 97%, 95%, 91%, 89%, and 88% accuracy, respectively, based on the classification results. The following is a summary of this article's primary contribution:

- The term "novel fuzzy set algorithm" refers to the combination of the level set fuzzy c-means (FCM) and the lesion region segmentation technique.
- The black widow optimization (BWO) algorithm is used to improve the classification performance of support vector machines (SVM).
- Images from five classes—psoriasis, paederus, herpes, melanoma, and benign—were gathered from the ISIC-2018 dataset.
- The suggested approach outperforms SVM, DCNN, DNN, and ANN in terms of classification accuracy.

2 Review of related works

Chatterjee et al. suggested an integrated computer-aided mechanism to detect skin conditions. The shape, color, texture, and irregular border of skin lesions were analyzed in order to extract various quantitative features prior to classification. Graylevel co-occurrence matrix (GLCM) and fractal-based regional texture analysis (FRTA) are used to quantify the textural information. The classification performance was assessed using the support vector machine and radial basis function. For BCC, dysplastic nevi, and melanoma classification, the experimental analysis yields 99.65%, 97.54%, and 98.99%, respectively; however, the feature dimensionality space is larger. Birkenfeld et al. developed the computer-aided classifier system to identify pigmented lesions that seemed suspicious. The authors chose 133 patients with a variety of skin lesions for this investigation. All lesions are examined by a board-certified dermatologist and classified as normal or abnormal based on the image. Depending on the testing set, a 100% sensitivity is attained for suspicious pigmented lesions. This computer aided classifier system is very useful for skin screening at the population level.

A naive Bayes (NB) classifier and dynamic graph cut algorithm (DGCA) were proposed by Balaji et al. for the segmentation and classification of skin diseases. The experimental datasets were selected from the International Skin Imaging Collaboration (ISIC) website (ISIC 2017) because they outperform the state-of-the-art methods like SegNet and FCN. Three different disease types were taken into consideration here: keratosis, melanoma, and benign cases. The thorough analysis shows that the classifications for keratosis, melanoma, and benign diseases are 92.9%, 91.2%, and 94.3%, respectively. Al-Masni et al. proposed the deep convolutional neural network (DCNN) classifier for the classification of skin conditions. The convolutional neural Med Biol Eng Comput network classifier consists of the DenseNet201, Inception-ResNet-v2, ResNet50, and Inception-v3. The boundaries of the skin lesions are separated from the full dermoscopy images by the full resolution convolutional network (FrCN). The performance analysis of convolutional neural network classifiers in the context of skin disease classification is conducted using the ISIC 2016, ISIC 2017, and ISIC 2018 datasets.

Multi-label classification methods were proposed by Chatterjee et al. to identify skin conditions like melanoma, BCC, nevus, and SK. For feature extraction, the cross-spectrum and cross-correlation approaches were presented. With the help of suitable kernel patches and comparable visual effects, both spectral and spatial feature extraction are explained. A multi-label ensemble multiclass skin lesion classification mechanism is used to classify skin lesions into three categories: epidermal, benign melanocytic, and benign melanocytic. Qin et al. developed generative adversarial networks (GANs) to categorize skin lesions. The GANbased data augmentation method improves the performance of skin lesion classification. By modifying the discriminator and generator, high-quality skin lesion images are produced. The performance of the skin lesion style-based GAN is assessed using quantitative evaluation metrics like recall, precision, inception distance (FID), and

inception score (IS). The experimental analysis yielded average precision of 96.6%, specificity of 74.3%, sensitivity of 83.2%, and accuracy of 95.2%.

A deep neural network (DNN) was proposed by Bajwa et al. for the identification of skin diseases. Images of skin diseases were selected from the ISIC Archive and DermNet datasets. The experimental results show improved accuracy and reproducibility. But it takes longer to execute. Zhang et al. proposed the DNN for the classification of skin diseases. Details of the dataset were supplied by the Union Medical College Hospital, and DNN's accuracy was 87.25%. The outcomes of the experiment show effective classification with increased computational complexity. Khan et al. proposed the deep neural network (DNN) as an efficient way to categorize skin conditions. Details of the image dataset are provided by dermoscopic datasets like ISBI 2016, ISBI 2017, and HAM 10,000. Good accuracy and improved reliability are attained based on the experimental results. But a better feature selection model was needed for this model. Numerous optimization techniques, including PSO, ABC, CS, and ACO, are used to solve the deep learning technique problems.

By employing implicit regularization through a two-phase training procedure, Qinghe Zheng et al. enhanced the deep CNN's capacity for generalization. To reduce overfitting and increase the DCNN's capacity for generalization, they employed regularization. The accuracy of their suggested approach was 76.23% for the ILSVRC2012 dataset and 76.64% for the CIFAR100 dataset. To optimize the DCNN, Zheng et al. introduced a layer-wise learning-based stochastic gradient descent (LLb-SGD) technique. A cross-media propagation mechanism is used to set an adaptive learning rate for every neural network layer. This method works with various datasets and architectures and is not affected by hyperparameters. To increase DCNN's capacity for generalization, Qinghe Zheng et al. [14] suggested a probably approximately correct (PAC) Bayesian framework based on the drop path technique. Using the generalization error boundary as a guide, this method shrinks the model size. The accuracy of their suggested approach was 96.80% for the CIFAR10 dataset and 81.4% for the ImageNet dataset.

Qinghe Zheng et al. provided a full stage data augmentation model for DCNN to increase its accuracy for natural image classification. The networks can be optimized and their capacity to generalize enhanced by the data augmentation carried out during the training and testing stages. The model's accuracy is 93.41% for the coarse-grained (CIFAR10) dataset and 70.22% for the fine-grained (CIFAR100) dataset. For automatic modulation classification, Qinghe Zheng et al. presented a spectrum interface based on two-level data augmentation testing in deep learning. At the testing stage, the data augmentation is calculated using a model ensemble. The majority voting system improves classification performance and stability. The suggested method, which uses data augmentation in both training and testing, has a classification accuracy of 58.75%. Table reviews the current approaches for classifying skin diseases.

Table 1 A literature review of skin disease classification

References	Methods	Name of the dataset	Advantages	Limitations	Accuracy
Chatterjee et al. [10]	RBF and SVM	Real-time dataset	The higher degree of accuracy and sensitivity at every stage	Higher feature dimensionality space	98.79%
Birkenfeld et al. [11]	Computer-aided classification	Dermatological databases	Low feature dimensionality with the fast screening process	Lower classification accuracy	75.9%
Balaji et al. [28]	DGCA and NB	ISIC 2017	Easy to implement the classifier with quick output prediction	Higher cost and complexity	94.3%
Al-Masni et al. [25]	DCNN	ISIC 2016, ISIC 2017, and ISIC 2018 datasets	Better classification performances with accurate results	The limited size of deep learning networks for both training and testing	98.79%
Chatterjee et al. [29]	Multi-label classification techniques	Real-time database	Malignant and benign lesions in the classes of melanoma, nevus, BCC, and SK have been identified.	Takes more processing time	98.79%
Qin et al. [30]	GANs	ISIC 2018 dataset	More accurate diagnostic decisions	Insufficient class-imbalanced data or labeled data	95.2%
Bajwa et al. [26]	DNN	DermNet and ISIC Archive datasets	Better reproducibility and accuracy	Takes more execution time	93%
Zhang et al. [31]	DNN	Union Medical College Hospital	Effectively classifies the dermoscopic images	Higher computational complexity	87.25%
Khan et al. [32]	DNN	ISBI 2016, ISBI 2017, and HAM 10000	Better reliability	Needs better feature selection model	89.8%
Zheng et al. [12]	DCNN	MNIST, CIFAR100, SVHN,USPS, and ILSVRC2012	Enhances the generalization capability of DCNN	Time-consuming and not reliable in high dimensional space	76.64%
Zheng et al. [13]	LLb-SGD, DCNN	CIFAR10 and ImageNet	Faster convergence and robust	The LLb-SGD technique needs frequent updates	-
Zheng et al. [14]	CNN	CIFAR10 and ImageNet	Higher model compression and lower accuracy loss	The drop path method used is not efficient for convolutional layers	81.4%
Zheng et al. [15]	DCNN	CIFAR10 and CIFAR100	Improves generalization capability and convergence	Needs higher training time and additional reasoning costs	70.22%
Zheng et al. [16]	DNN	RadioML 2016.10a dataset	Can be efficient for large-scale augmentation and can be directly applied in cognitive radios	Low accuracy	58.75%

3 Proposed approach

This study shows how various skin lesions, including psoriasis, paederus, herpes, melanoma, and benign, are categorized. Image pre-processing, lesion area segmentation, feature extraction, and classification are the processes that go into identifying skin lesions. The proposed methodology's workflow diagram is shown in Fig 1

3. 1 Pre-processing

The input image is first preprocessed using the semi-automated image preprocessing method. Raw images are fed into camera-specific software, which then converts them to the Tagged Image File Format (TIFF). A single lesion in the input image with a diameter larger than 3 mm is manually clipped and saved separately. Dermoscopic images were obtained for this analysis using a variety of dermoscopic conditions and lighting setups. Because the gray world constancy algorithm is used for normalization, the images have color variance and irregular lighting is corrected. One unfavorable consequence of image processing is image noise. A digital camera's sensors misalign as light strikes the lens, producing noise. Only a few types of image noise are inevitable, even if they are clearly visible. Gaussian noise affects the input and is eliminated during the pre-processing phase by applying the Wiener filter. Color standardization and image acquisition with noise reduction are done during pre-processing in order to prepare the image for subsequent processing.

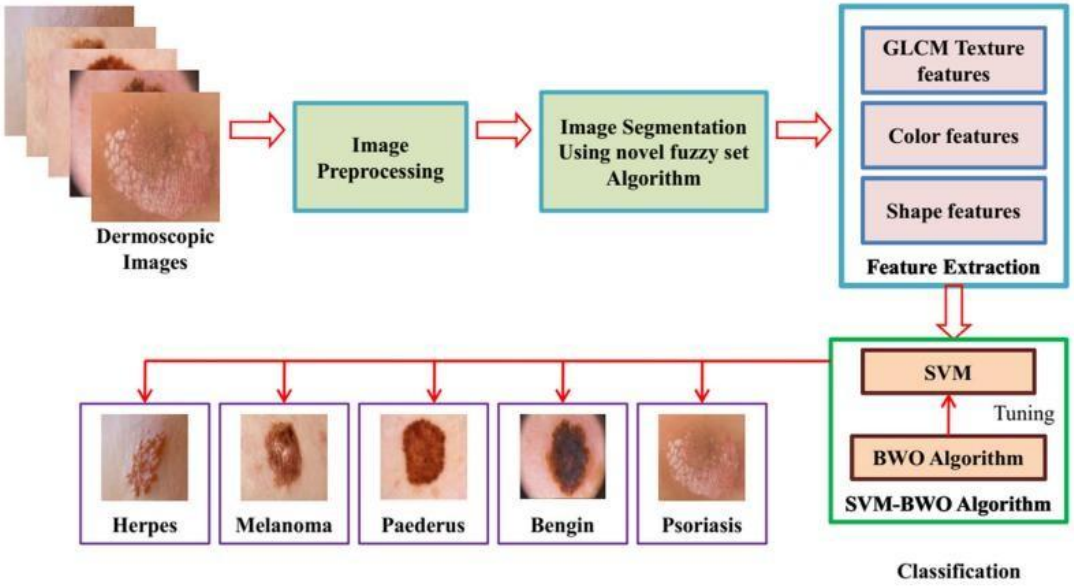

Fig 1.

3.2 Image segmentation using novel fuzzy set algorithm

Following pre-processing, the novel fuzzy set algorithm is used to precisely segment the lesion regions. The intermediate morphological operations are removed because adaptive optimization for fuzzy clustering necessitates spatial information. The main driver behind the computation models that are used for any dimension problem is the combination of fuzzy cmeans (FCM) algorithms and level sets. It is possible to obtain the advantage of particular circumstances through image segmentation for improved performance. The new fuzzy level set algorithm is suggested for segmenting the skin lesion region. We estimate the level set evolutions regularized with the controlling parameters. The image segmentation scheme's distinct phases are shown.

In the presence of new fuzzy level set algorithms, level set segmentation initialization and parameter configuration are automated through the use of spatial fuzzy clustering. Spatial and FCM constraints are used to approximate the contours of interest in the medical images. Better level set functions use the initialization of flexible to achieve the FCM results, as illustrated in Fig 2.

$$\emptyset_0(a,b) = \begin{matrix} -D, & \emptyset_0(a,b) < 0 \\ D & else \end{matrix} \quad \{ \qquad (1)$$

,

where $\emptyset_0$ is the level set function and the initial contour is $\emptyset_0(a, b)$ with the customizable constant D. Hence, $S_k : \{s_k = {}_{mk}$, m = a × M_b + b} is the interest component in FCM results, and the level set function is initiated as follows:

$$\emptyset_0(a, b) = -4\psi(0.5 - X_k) \qquad (2)$$

From Eq. (2) the constant regulating the Dirac function is . Equation (3) explains the Dirac function.

$$\delta(a) = \begin{cases} 0, & |a| > \psi \\ \frac{1}{2\psi}\left[1 + \cos\left(\frac{\pi a}{\psi}\right)\right], & |a| \le \psi \end{cases} \qquad (3)$$

Here, the binary image X_k is obtained using Eq. (4). The adjustable threshold is $x_0 \in (0,1)$.

$$X_k = S_k \ge x_0 \qquad (4)$$

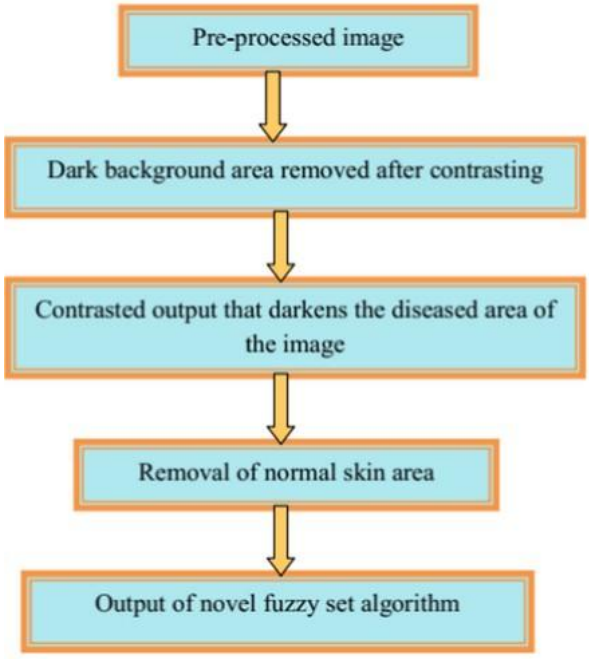

Fig 2.

Importance	Parameters
Level set evolution with maximum iteration	T
Level set evolution of time step	γ
Artificial balloon force	u
Contour length coefficient for smoothness regulation	ρ
Penalty term $\zeta(\phi)$ of the weighting coefficient	η
The initial set function with the gradient strength controlling	D
Gaussian smoothing function of spread controlling	σ
Regulator for Dirac function $\delta(\phi)$	ε

Convergence behaviors, the numerical cost of level set methods, and other controlling parameters are linked to the level set methods in Table 2, which is crucial for the segmentation of skin lesions. The conventional or generalized Hamilton-Jacobi level set technique can be enhanced by adding a regularized/hole nucleation technique to the optimization scheme. Nevertheless, this process is frequently intricate and necessitates multiple factors.process is frequently intricate and calls for a number of factors. It's crucial to set them up roughly because, regrettably, this differs from case to case. The configuration of these parameters is governed by a few fundamental rules.For the proper level set segmentation, a lot of general guidelines are used through trial and error. The time step product and penalty coefficient ($\gamma \times$) must be less than 0.25 for stable evolution. The parameter D is higher when compared to 2 . Boundary leakage risks have materialized, and the level set evolution down has revealed a larger value of D. Therefore, a larger u accelerates the evolution of the level set. The aforementioned recommendations are crucial for segmenting the lesion region, but they are insufficient to forecast the ideal setup.

According to Eq. (2), the initial level set function $\emptyset_0$ is convenient to determine the are β and length ℓ.

$\beta = \int_1 G(\phi_0)dadb$ (5) $\ell = \int_1 \delta(\phi_0)dadb$ (6)

where $G(\phi_0)$is the Heaviside function.

$$G(\emptyset_0) = \begin{cases} 1\,, & \phi_0 > 0 \\ 0\,, & \phi_0 < 0 \end{cases} \quad (7)$$

If the interest variable is larger, we observe level set evolution, and the larger ratio is denoted as follows:

$$\beta / = \ell \quad (8)$$

In the fuzzy set algorithm, reasonably allocate the time step γ and. The following equation sets the penalty coefficient.

$$= 0.2/ \quad (9)$$

For stable evolution, the product ($\gamma \times$) is lower than 0.25. From the FCM Eq.(2), we obtain the initial level set function $\emptyset_0$.

$$\rho = 0.1 \quad (10)$$

Where ρ is the contour length coefficient for smoothness regulation. The Mamdani fuzzy inference rule is used in our fuzzy technique. The two laws governing the balloon force's level set evolution are u.

(i) **IF** the expansion means negative **THEN** the shrinkage means positive signs in which level set function with advancing direction is determined using the sign.

(ii) **IF** the fatter level set evolves **THEN** the value u is larger.

Set the controlling parameter u as the global constant in the standard level set function, which makes the faster level set function. When ϕ is beyond the genuine boundary, the direction of the level set function is changed automatically. The quantitative index to regularize the level set function and the initial FCM segmentation is determined. The membership degree of each image pixel ηk is taken with a novel fuzzy set algorithm. Equation (11) explains the improved balloon force.

$$H(S_k) = 1 - 2S_k \quad (11)$$

At each image pixel, the variable pushing or pulling force with the balloon force output matrix is $H(S_k)(\in [-1, 1])$. According to FCM , the image gradient information incorporates (h, ϕ) as given below:

$$\zeta(h, \phi) = \gamma\delta(\phi)\left(h\frac{\nabla\phi}{|\nabla\phi|}\right) + uh\delta(\phi) \quad (12)$$

Equation (12) is rewritten as follows:

$$\zeta(h, \phi) = \gamma\delta(\phi)div\left(h\frac{\nabla\phi}{|\nabla\phi|}\right) + hH(\phi S_k)\delta(\phi) \quad (13)$$

The improvement of image segmentation provides many functional advantages. According to the spatial fuzzy clustering algorithm, the balloon force is directly derived. The distance to the genuine object adapts to the level set evolution. Stabilize the level set evolution automatically because the conservative ρ is presumed. For robust segmentation, the flexibility selects the larger evolution iteration T. In order to avoid excessive or insufficient segmentation, the operator keeps an alert to the level set evolution without enhancement.

3.3 Feature extraction

This section involves extracting the segmented lesion image's shape, color, and texture features. Below is a detailed explanation of the asymmetry, color, and texture feature extraction procedure.

3.3.1 Asymmetry feature extraction

The majority of the pictures of skin lesions are asymmetrical. If we use the line to categorize the segmented region, the two parts will never match. Skin doctors say that benign and melanoma grow asymmetrically. The asymmetry value is calculated by subtracting the segmented shape area on the axis design side. The two area differences that result are explained by equation (14).

$$A_{symmetry} = \left(\frac{A_{min}}{A_{total}}\right) * 100 \quad (14)$$

According to Eq. (14), A_{min} has the lowest absolute difference value among the different subregions of the provided input image. A_{total} is the shape of the skin lesion that was found. The asymmetry of the skin lesion region is calculated by locating the gravity center of the preprocessed skin input image. Eq. (15) is used to measure the dimensionless symmetricity between bulkiness (B).

$$B = \frac{Equivalent\ Ellipse\ Area}{Original\ Area} \quad (15)$$

An analogous inertia moment is occupied by the image of the skin lesion. The bulkiness value of skin lesions indicates that nearly 75.5% of them are malignant. The geometric asymmetry is calculated by splitting the skin lesion into two sections. The spaces (0, a, b) are used to represent each of the skin lesion's points. The symmetry rate for the provided input image is determined in the steps below.

(i) The creation of object rotation is followed by two principle axes.

(ii) Draw a line connecting the original image and the thought object.

3.3.2 Color Feature Extraction

Tan tones, black and brown hues, and red or blue spots are characteristics of melanocytotic lesions. Color descriptors describe different color features or properties involved inside the lesion. Additionally, color descriptors from various color channels—like color and standard deviation—are taken into account. The color descriptors that were extracted from the segmented image are explained in the section that follows.
The average color value is given by the mean.

$$\mu = \frac{1}{M}\sum_{k=1}^{M} R \qquad (16)$$

The square root of the variation is the standard deviation (SD).

$$\sigma = \sqrt{\frac{1}{M}\sum_{k=1}^{M}(R_k - \mu)^2} \qquad (17)$$

The asymmetry degree is determined using skewness.

$$S_{kewness} = \sqrt[3]{\frac{1}{M}\sum_{k=1}^{M}(R_k - \mu)^3} \qquad (18)$$

The variance is given as below:

$$V_{ariance} = \frac{1}{M}\sum_{1}^{M}(R_k - \mu)^2 \qquad (19)$$

where M represents the total sample size, R represents the color channel of the image at a specific pixel, and μ is the mean value. Equations (16) and (17) were used to calculate the color distribution characteristics. Color indexing plays a vital role in this study.

3.3.3 Texture feature extraction

The gray-level co-occurrence matrix (GLCM) is a histogram of co-occurring grayscale pixel values at the specified offset over the segmented input image. We extract the homogeneity, energy, contrast, and correlation parameters from the GLCM. GLCM is used to extract the skin pixels, which include RGB (red, green, and blue), HSV (hue, saturation, and value), and YCbCr (luminance and chrominance) color models. For an image X of size M×M, the GLCM is created as follows: It calculates the distance and angular relationship between the pixels in the particular region.

$$R(j,k) = \sum_{j=1}^{M}\sum_{k=1}^{M}\begin{cases}1, & r(a,b) = j \text{ and } X(a + \Delta a.\, b + \Delta b) = k \\ 0 & Or\ else\end{cases} \qquad (20)$$

The joint probability of intensities j and k is R(j,k) at any point and is defined using Δa and Δb, where a and b represent the particular position in the image, Δa represents the angle between pixels, and Δb represents the distance between pixels.

(i) The element distribution in the matrix closeness is determined using the homogeneity parameter.

$$H_{omogenetity} = \sum_{j,k}\frac{R(j,k)}{1+|j-k|} \qquad (21)$$

(ii) The sum of squared features in the GLCM corresponds to the angular second moment or energy.

$$E_{nergy} = \sum_{j,k} R(j,k)^2 \qquad (22)$$

(iii) The local variations present in the co-occurrence conditions are measured with the help of the contrast parameter.

$$C_{ontrast} = \sum_{j,k}|j-k|^2 R(j,k) \qquad (23)$$

(iv) The possibility incidences of the identified pixel pairs are presented using correlation.

$$C_{orrelation} = \sum_{j,k}\frac{(j-\mu j)(k-\mu k)R(j,k)}{\sigma_j \sigma_k} \qquad (24)$$

where σ_j *and* σ_k are the standard deviation values of j and k, respectively. From the segmented image region, one of the influential tools is GLCM to extract image features. From the segmented image region, another interesting feature such as entropy is extracted. The differences among the two nearby pixels are similar if R_j represents the probability.

$$E_{ntropy} = -\sum_{j,k} R_j(log_2 R_j) \qquad (25)$$

The correct regularity rate of the image is inferred at the end of the procedure by taking maximum values. The classification operation is performed once the entire features are extracted. Finally, the shape, color, texture, and asymmetry features are effectively extracted from the segmented image. For classification, the GLCM, color, shape, and texture features are extracted. From each segmented image, the entropy, homogeneity, energy, correlation, and contrast information features are extracted.

3.4 Classification

These features are then fed into the classification process after feature extraction. The support vector machine (SVM) is used in this study for the classification process; therefore, the black widow optimization (BWO) algorithm is used to adjust the parameters in SVM. The resultant newly created classification method is known as the SVMBWO algorithm. Below is an explanation of each step in the SVM-BWO algorithm for classifying skin diseases.

3.4.1 Black widow optimization algorithm

The black widow optimization (BWO) algorithm is described in this section. Spiders are airbreathing arthropods with eight legs and poisonous fangs. Out of all the orders of organisms, these species belong to the largest arachnid order. Famous black widows are members of the spider subfamily Latrodectus because of their highly neurotoxic venom potential. The term "black widow" refers to the female spider. Black widows' way of life is influenced by Black widow optimization (BWO). The subsequent subsection lays out the BWO algorithm's sequential procedure. Initialization of the population In order to solve the optimization problems, the problem value variables must form a suitable structure for the current problem. These structures are referred to as particles and chromosomes in PSO and GA terminology. The black widow spider thinks about each problem's possible solution. Each black widow spider represents the values of the problem variables. To solve the benchmark functions, the structure needs to be viewed as an array .The widow array of $1 \times M_{variables}$ in a $M_{variables}$ dimensional optimization problem represents the solution problem. The black widow arrays are explained by equation (26).

$$Windowes = [z1, z2, z3, \dots , zMvariables] \quad (26)$$

where , $(z_1, z_2, z_3, \dots , z_{Mvariables})$ is the floating number of each variable value. In this work, the black widow fitness f is evaluated as shown below.

$$f = f(z_1, z_2, z_3, \dots , z_{Mvariables}) \quad (27)$$

The initial population with the candidate widow matrix size $M_{population} \times M_{variable}$ is generated to start the optimization algorithm.

Make off Parent pairs are selected at random to carry out the procreating step through mating. The male Black widow is eaten by the female during or after that. Since the pairs are independent of one another, they begin mating to create the next generation.

Approximately 1000 eggs are produced in each match. Fewer spider babies survived in the end. The gamma array is created, and the offspring is produced by this gamma.

According to Equation (28), the parents are represented by z_1 and z_2 , and the offspring γ are x_1 and x_2.

$$\begin{cases} x_1 = \gamma \times z_1 + (1 - \gamma) \times z_2 \\ x_2 = \gamma \times z_2 + (1 - \gamma) \times z_1 \end{cases} \quad (28)$$

The procedure is carried out $M_{variables}/2$ times if the randomly chosen numbers are not duplicated. Ultimately, the children and mother are merged into new arrays and arranged according to their fitness value. According to the cannibalism rating, only a small number of the best individuals are fed to the newly created population.

Cannibalism The BWO contains three different forms of cannibalism, which are described as follows:

- Sexual cannibalism occurs when a female Black widow consumes the male Black widow during or after mating. The fitness values of both males and females are acknowledged.
- Sibling cannibalism occurs when strong spiderlings consume their weaker siblings. The cannibalism rating is set to C_R based on the number of survivors.
- The third type of cannibalism is frequently seen when the young spiders consume their mother. The fitness value is used to identify the strong and weak siblings.

Convergence and mutation The Mutepop numbers of people are chosen at random from the population. Each of the solutions chosen at random exchanges two elements in the array. Lastly, a predetermined number of iterations are known as stopping criteria, and it is thought that no trade observance in the fitness value of the

best widow reaches a certain level of accuracy over multiple iterations. The general steps of BWO are described in Algorithm 1.

3.4.2 Support vector machine tuning based on BWO (SVM-BWO)

Support vector machines (SVM) are a popular machine learning algorithm used to solve optimization problems. This part, which is tailored for large-scale learning, is the focus of the linear SVM. SVM is used to perform complex tasks in a variety of domains, including image classification, sensor multi-fault diagnosis, disease prediction, and monitoring metal-oxide surge arrester conditions.The SVM solves both linear and non-linear problems and is frequently used for many real-world applications. However, the target classes overlap, and the SVM is not appropriate for datasets. The SVM will crash if each data point has more features than there are training data samples. In order to improve SVM's performance in terms of regularization, loss function, and kernel during classification, we employed BWO. The SVM-BWO algorithm's performance in classifying diseases in images is shown in Figure 3.The hyperplane is used to split the training data into the five classes of skin diseases in order to train the SVM.

Algorithm 1: Pseudocode of BWO algorithm

Initialization of black widows, procreating, cannibalism, and mutation rates with a maximum number of iterations.
Initialize black widow spider populations with D-dimensional widow array
Calculate the number of reproduction (Rp) based on the procreating rate
Choose the relevant solutions Rp from the population and store this in Population-1
For $j = 1$ **to** Rp ***do***
    From population-1, randomly choose two parent solutions
    Equation (28) generates the children
    Father is destroyed
    Destroy few children according to the cannibalism rate
    The balance solutions are stored in the Population-2
End For
    Compute the number of mutation *nm* children depending upon the rate of cannibalism
For $j = 1$ **to** nm ***do***
    Choose the solution from Population-1
    Randomly mutate the widow and create the new solution
    The new solution is store in Population-3
End For
    Update Population=Population-2+Population-3

The support vectors, which are typically a subset of the training set's vectors, are primarily used to represent them. The SVM's ability to make decisions can be improved by determining which vectors were chosen as support vectors. . Assume that the training vectors for the two classes are vectors $x \in \Re^l : x_j = \{1, -1\} and\ y_j \in \Re^l$, $J = 1, \ldots, l$. A linear classifier is used to generate the weight vector (W). Eq. (29), therefore, provides an explanation of the decision function.

$$sgn(W^T y) \tag{29}$$

The following primal problems are solved by the L2- regularized L1-loss support vector classifier.

$$\min_W \tfrac{1}{2} W^T W + D \sum_{j=1}^{l} \left(\max\ \left(0, 1 - x_j W^T y_j\right)\ \right) \tag{30}$$

Where

$$min_\beta\ \tfrac{1}{2}\ \beta^T \overline{P}\ \beta - e^T \beta \tag{31}$$

Subject to $0 \le \beta_j \le V, j = 1, \ldots, l$

Where $P_{jk} = x_j x_k y_j^T y_k$ and the vector of all ones are e and the diagonal matrix is
$\bar{P} = P + d$.
$For\ L1 - loss\ SVC : d_{jj} = 0\ for\ all\ j\ and\ V = d$
$For\ L2 - loss\ SVC : d_{jj} = \tfrac{1}{2}d\ for\ all\ j\ and\ V = \infty$ (32)
The sparse solution W is generated by L1-regularization. The below primal issue is solved using L1-regularizedL2- loss SVC.

$$\min_W ||W||_1 + D \sum_{j=1}^{1} \left(max\left(1 - x_j W^T y_j\right)\right)^2 \tag{33}$$

where the penalty parameter is D > 0 and ‖·‖1 represents the 1-norm.

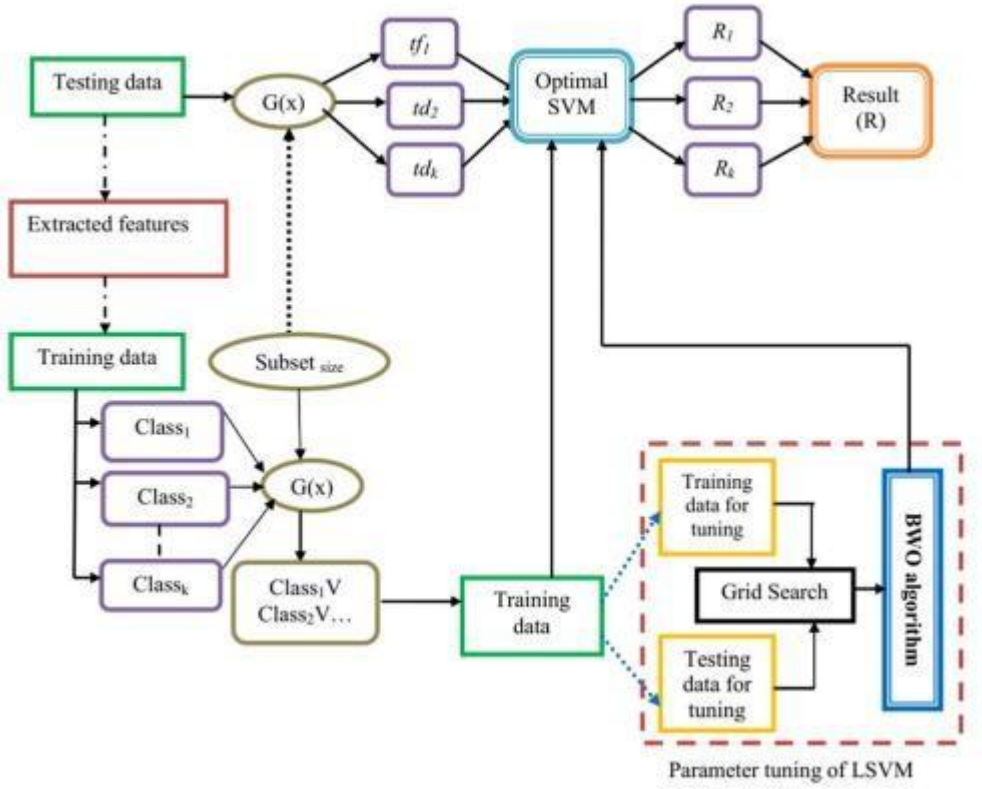

Fig. 3.

SVM-BWO effectively improves the classification accuracy for linear SVM training by choosing the penalty or cost parameter of error term D. The initial value D is predefined by the cross-validated grid search. The SVM-BWO is represented by the red, region-bounded rectangle. The training data size selection is applied to the subset of split testing data. Lower accuracy results from a significant reduction in the time and computational effort needed to train classifiers. A majority voting ensemble, denoted by DL{m} _ SVM – BWO and the number of classifiers m in which the classification performances are improved for SVM-BWO, extends this methodology. Additionally, the SVM-BWO can be used for binary and multi-class tasks. The random vectors are denoted by R1 and R2 in Fig. 2. The number of classes is D, where k is the different number of classes, and the inertia coefficients are W. Lastly, using training and testing data, the SVM-BWO algorithm efficiently classifies the diseases according to pertinent disease classes. Algorithm 2 outlines the steps of the suggested SVM-BWO algorithm for classifying skin diseases.

4 Results and discussion

The suggested work performance in terms of classifying skin diseases is validated in this section. The suggested model's implementation process is managed in MATLAB 2020a using an Intel ® i7-4070. The performance of the suggested work is examined using a variety of performance analysis techniques and cutting-edge comparisons.

Algorithm 2: Pseudocode of SVM-BWO for skin disease classification

Input: The skin disease image is taken from ISIC-2018 and HAM 10000 datasets
Output: Image with a disease label
Step 1: Image preprocessing with noise removal and color standardization
Step 2: A novel fuzzy set algorithm for lesion segmentation
Step 3: Extraction of shape, color, and texture features
Step 4: Optimize the SVM architecture using the BWO algorithm (discussed in Algorithm 1) for skin disease classification
    For each image (*i*) present in the dataset
        Output disease label (i) in the BWO optimized SVM architecture
    End For

This dataset includes a variety of skin conditions. We selected five types of skin diseases from this dataset, using 2565 training sample images and 905 testing sample images. The list of training and testing parameters is shown in Table 3.
Additionally, Fig. 4 shows the sample images with the results of segmentation and classification.

Description	Name of the skin diseases					
	Healthy	*Psoriasis*	*Paederus*	*Herpes*	*Melanoma*	*Benign*
Total number of samples	2014	275	427	348	276	130
Training samples	1567	185	317	214	186	96
Testing samples	447	90	110	134	90	34

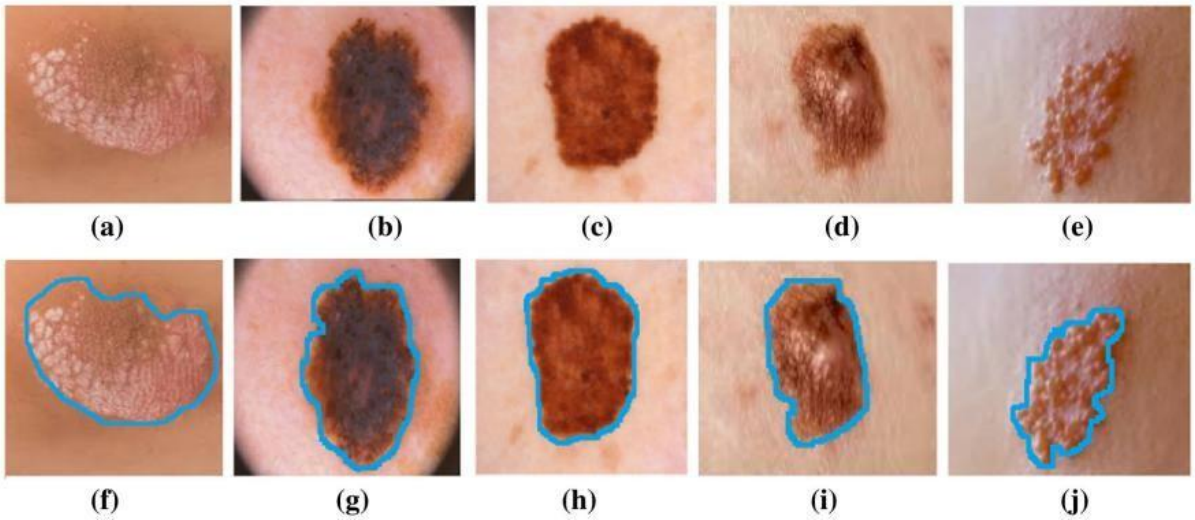

Fig. 4 Sameples images with segmentation and classification outputs:
a, f psoriasis; **b, g** paederus; **c, h** herpes; **d, i** melanoma; and **e, j** benign

4.2 Evaluation measures

This study analyzes classification performance using the following metrics: accuracy, specificity, sensitivity, dice score, precision, and recall.

$$Accuracy = (tp + tn)/(tp + fp + tn + fn) \quad (34)$$

$$Specificity = tn/(tn + fp) \quad (35)$$

$$Sensitivity = tp/(tp + fn) \quad (36)$$

$$D_{ice}S_{core} = \frac{2tp}{((fp+tp)+(tp+fn))} \quad (37)$$

$$P_{recision} = tp/(tp + fn) \quad (38)$$

$$R_{ecall} = tp/(tp + fn) \quad (39)$$

where tp is true positive based on healthy images categorized as healthy, tn is true negative based on unhealthy images categorized as unhealthy, fp is false positive based on healthy images categorized as unhealthy, and fn is false negative based on unhealthy images categorized as healthy.

4.3 Performance analysis

Table 4 shows the dice score performance for segmenting images of skin diseases. This experiment makes use of the fuzzy cmeans (FCM) algorithm, Otsu, DGCA, modified level-set (MLS), and the suggested approach. This investigation shows that the suggested segmentation model outperforms current techniques in terms of segmentation results.
Table 5 formulates the texture features based on different skin disease performances.
Energy, uniformity, entropy, correlation, and contrast parameters are used to choose the texture feature from the segmented skin image. For this experiment, we use five skin diseases along with these parameters' maximum and minimum values. Below is an evaluation of the five skin disease types with regard to GLCM

texture feature performances. Psoriasis, paederus, herpes, melanoma, and benign achieve energy values of 205.103, 121.507, 345.289, 1437.6, and 873.670 at their highest.
The maximum uniformity values for psoriasis, paederus, herpes, melanoma, and benign conditions are 3.450, 3.294, 3.290, 3.923, and 3.902. Psoriasis, paederus, herpes, melanoma, and benign conditions provide values that are 0.5663, 0.1267, 0.5634, 0.3026, and 0.3890 higher than the minimum entropy values for maximum entropy. Additionally, psoriasis, paederus, herpes, melanoma, and benign conditions yield maximum uniformity values of 40.289%, 87.987%, 178.345, 188.098, and 89.006%.
The efficiency of feature extraction in terms of color, texture, and symmetry is displayed in Figure 5. The segmented image's color, GLCM texture, and asymmetry features were extracted for this work, and the accuracy, specificity, and sensitivity of these features are calculated. The color feature offers 95% sensitivity, 91% specificity, and 90% accuracy.
Likewise, GLCM texture features yield 70% accuracy, 72% specificity, and 68% sensitivity. The asymmetry features show 80% sensitivity, 82% specificity, and 80% accuracy.

The classification accuracy for different types of skin diseases is shown in Fig. 6. Table 3 plots the total number of images for each category. This study selects 2014 healthy photos with 275 cases of psoriasis, 427 cases of paederus, 348 cases of herpes, 276 cases of melanoma, and 130 benign cases. This yields the following representation of each category's accuracy value. Therefore, 100%, 97%, 95%, 91%, 89%, and 88%, respectively, are the classification accuracy for healthy, psoriasis, paederus, herpes, melanoma, and benign conditions.

Table 4 Performances of segmentation using dice score value

Name of the methods	DGCA	Otsu	FCM	MLS	Proposed
Dice score values	0.803	0.794	0.807	0.790	0.825

4.4 Comparative analysis

The convergence efficiency in relation to cutting-edge methods is shown in Figure 7. Various algorithms with varying numbers of iterations and populations are employed here, including the genetic algorithm (GA), ant bee colony (ABC), ant colony optimization (ACO), particle swarm optimization (PSO), and black widow optimization (BWO). In the case of unimodal test functions, the search algorithm and its rate of convergence are more significant than the final results. The suggested BWO produces desired results at a faster rate of convergence than the other approaches. Because algorithms like GA, ABC, ACO, and PSO frequently become stuck in local minima and have limited exploration capabilities, the FBWO algorithm performs better in terms of convergence. Compared to other approaches, the BWO has a faster global optimum and a higher rate of convergence (Fig. 6). Table 6 provides an explanation of the algorithm's run time during the training and testing stages.

Table 5 Performances of texture features based on various skin diseases

Parameters		**Name of the skin diseases**					
		Healthy	***Psoriasis***	***Paederus***	***Herpes***	***Melanoma***	***Benign***
Energy	Min	23.23	36.923	52.218	93.0058	843.782	234.48
	Max	103.13	205.103	121.507	345.289	1437.6	873.670
Uniformity	Min	1.647	3.0617	2.945	2.673	2.790	3.082
	Max	2.50	3.450	3.294	3.290	3.923	3.902
Entropy	Min	0.023	0.1823	0.0742	0.1355	0.2951	0.2891
	Max	0.103	0.5663	0.1267	0.5634	0.3026	0.3890
Correlation	Min	1.005	1.8731	2.8167	3.5303	3.6721	3.2489
	Max	2.230	3.6723	3.2025	3.7892	3.9827	3.7201
Contrast	Min	7.703	8.713	51.672	41.786	67.922	35.959
	Max	31.20	40.289	87.987	178.345	188.098	89.006

The state-of-the-art comparison based on segmentation results is plotted in Figure 8. Using other cutting-edge techniques such as the dynamic graph cut algorithm (DGCA), full resolution convolutional network (FrCN), Otsu's method, and watershed algorithm, this experiment verifies the segmentation performance of the suggested novel fuzzy set segmentation algorithm. The suggested innovative fuzzy set segmentation algorithm shows superior segmentation results when compared to the current techniques. Fig. 9 displays a state-of-theart comparison based on classification results. Using classification metrics like accuracy, specificity, sensitivity, precision, and recall measure, we have chosen four cutting-edge techniques for this experiment: RBF and SVM,

DCNN, DNN, artificial neural network (ANN), and the suggested SVM-BWO algorithms. The suggested SVM-BWO only achieves better performance metrics when compared to all other approaches. As a result, the suggested SVMBWO approach exhibits 92% accuracy, 90% specificity, 78% sensitivity, 80% precision, and 76% recall. In any case, the suggested SVM-BWO performs better in classification than alternative techniques.
The suggested fuzzy level set algorithm's segmentation performance is assessed by contrasting it with alternative methods like DGCA-NB, DCNN, GAN, and DNN. The generalization error comparison results for the various methods, as well as the training and testing times, are shown in Table 7. It is evident from Table 7's results that the SVM provides better segmentation accuracy than the DGCA-NB, DCNN, GAN, and DNN approaches.

The computational complexity of the DCNN, GAN, and DGCA-NB techniques is the primary cause of their higher error rates and time complexity. Thus, it can be said that the fuzzy level set algorithm performs better in segmentation than the others.

4.5 Discussion

The results of the segmented scar tissue and the skin disease-affected image are shown in Figure 4. Both the benign and malignant skin images show a single layer of scar tissue. Because of the irregular and deficient boundaries, it is thought to be a difficult task to separate the cancerous tissues from the skin. FCM-based clustering performs better than alternative techniques in terms of level set initialization, despite the challenge of figuring out the precise level set parameters and ideal initialization. The suggested fuzzy level set algorithm seems to be effective in segmenting the medical image without defined boundaries because it is always necessary to track the motion of level set contours

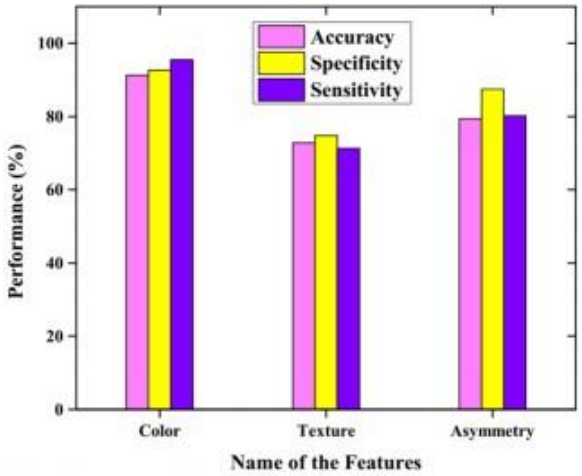

Fig. 5 Feature extraction performances

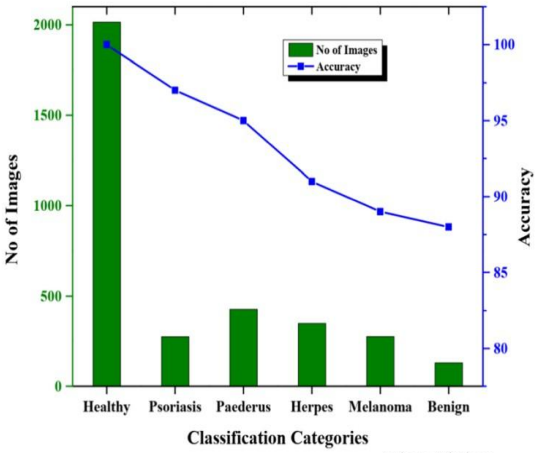

Fig. 6 Classification performance with respect to the accuracy

In the majority of situations, the fuzzy level set algorithm produces accurate results and automatically determines the controlling parameters for fuzzy clustering. For image segmentation, the fuzzy level set algorithm is therefore a great option. The quantity of training samples used determines the effectiveness of both neural networks and deep learning methods. The instances found in the training dataset are used to assess the SVM's segmentation performance.
Table 8 shows the SVM technique's generalization performance in terms of generalization error as well as the training and testing times. Additionally, the suggested approach is contrasted with deep neural networks (DNN) and artificial neural networks (ANN). Because there are fewer training samples for the ANN and DNN than for the other methods, they exhibit greater generalization errors. When compared to the ANN and DNN, the generalization error is low for the suggested technique because the SVM technique can provide high accuracy and low generalization error even with a small number of training samples.

Table 6 The run time of the algorithm in both of the training and testing phases

Learning	Name of the algorithms	Training time (ms)	Testing time (ms)
Original	GA	110	94
	ABC	103	95
	ACO	123	102
	PSO	99	80
	FBWO	94	79
First iteration	GA	15	140
	ABC	112	197
	ACO	33	132
	PSO	87	176
	FBWO	16	78
Second iteration	GA	32	143
	ABC	36	156
	ACO	33	149
	PSO	30	145
	FBWO	29	132

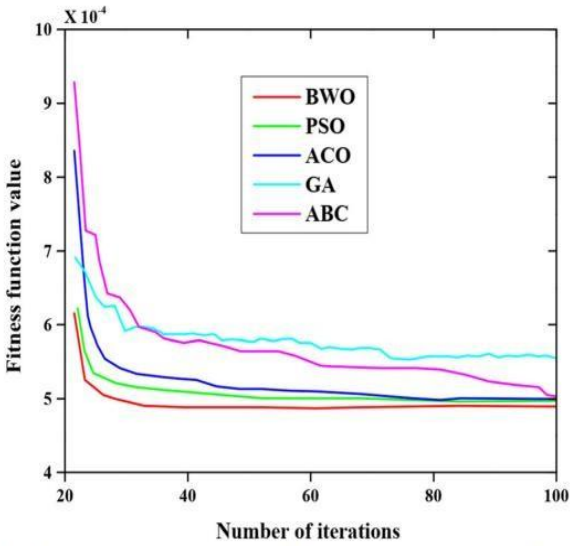

Fig. 7 Convergence performance with respect to state-of-the-art methods

5 Conclusion

SVM-BWO was proposed in this paper for the classification of skin diseases. MATLAB 2018 software is used to implement the suggested model. Five skin conditions are selected, each with a healthy image: psoriasis, paederus, herpes, melanoma, and benign. The section above contains a tabulation of the quantity of training and testing images. Psoriasis, paederus, herpes, melanoma, and benign diseases achieve optimal maximum and minimum values in energy, uniformity, entropy, correlation, and contrast features during feature extraction.

The classifications of benign, psoriasis, paederus, herpes, melanoma, and healthy yield 100%, 97%, 95%, 91%, 89%, and 88% accuracy, respectively. Compared to PSO, ABC, ACO, and GA methods, BWO has a higher and superior convergence rate. Measures of accuracy, specificity, sensitivity, precision, and recall are all improved by the suggested approach. We will investigate the data balancing effect for multi-class disease classification in the future. Medical practitioners can use the proposed work to detect skin abnormalities early and provide timely, appropriate treatment.

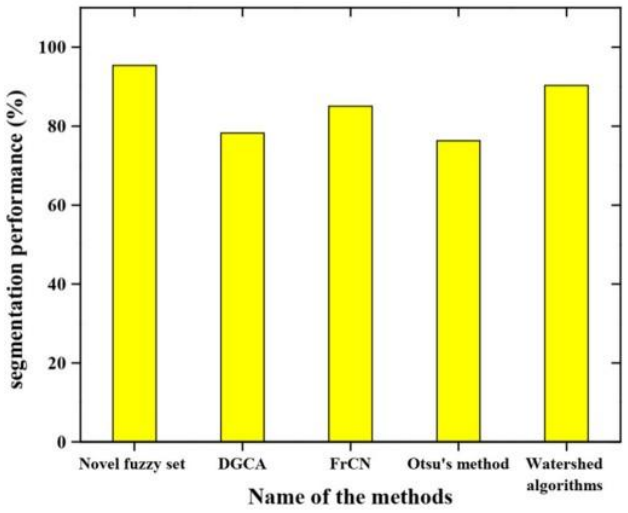

Fig. 8 State-of-the-art comparison based on segmentation results

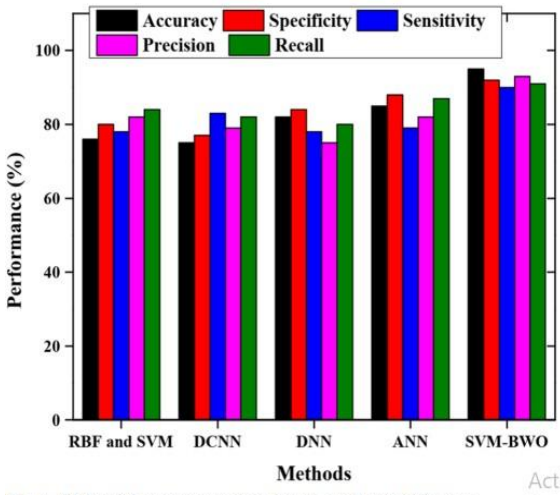

Fig. 9 State-of-the-art comparison based on the classification

Table 7 Generalization performance comparison for segmentation techniques

Technique used	Training time (ms)	Testing time (ms)	Overall time taken for computation (ms)	Error rate (%)
DGCA-NB [28]	325	154	479	3.25
DCNN [25]	761	412	1173	4.01
GAN [30]	654	352	1006	3.35
DNN [26]	456	159	615	2.36
Proposed fuzzy level set algorithm	189	78	196	1.14

Table 8 Comparison in terms of generalization performance

Number of samples used for training	SVM				ANN [33]			DNN [17]		
	Training time (ms)	Testing time (ms)	Number of support vectors	Generalization error (%)	Training time (ms)	Testing time (ms)	Generalization error (%)	Training time (ms)	Testing time (ms)	Generalization error (%)
100	875	15	13	1.02	1365	38	3.56	1245	35	3.21
200	1121	28	25	1.15	1398	45	3.21	1256	30	3.42
500	1130	38	33	0.98	1458	60	3.57	1278	58	3.56
1000	1139	50	89	0.96	1478	79	3.96	1296	77	4.01
2000	1145	72	117	0.94	1514	89	3.24	1300	80	4.15

Data availability Data sharing is not applicable to this article as no new data were created or analyzed in this study.

Declarations

Ethical approval: This article does not contain any studies with human participants or animals performed by any of the authors.

Informed consent: Informed consent was obtained from all individual participants included in the study.

Conflict of interest: The authors declare no competing interests.

References

1. Chaurasia V, Pal S (2019) Skin diseases prediction: binary classification machine learning and multi model ensemble techniques. Res J Pharm Technol 12(8):3829–3832
2. Wei L-s, Gan Q, Ji T (2018) Skin disease recognition method based on image color and texture features. Computational and mathematical methods in medicine 2018:1–10
3. Verma AK, Pal S, Kumar S (2019) Classification of skin disease using ensemble data mining techniques. Asian Pac J Cancer Prev: APJCP 20(6):1887
4. Brinker TJ, Hekler A, Utikal JS, Grabe N, Schadendorf D, Klode J, Berking C, Steeb T, Enk AH, von Kalle C (2018) Skin cancer classification using convolutional neural networks: systematic review. J Med Internet Res 20(10):e11936
5. Ye J, Wang G, Tan J, Zheng J, Zhang X, Xu F, Cheng S, Chen Z, Zhang W, Liao Y (2019) Identification of candidate genes involved in anthocyanin accumulation using Illumina-based RNA-seq in peach skin. Sci Hortic 250:184–198
6. Sundararaj V (2019) Optimised denoising scheme via oppositionbased self-adaptive learning PSO algorithm for wavelet-based ECG signal noise reduction. Int J Biomed Eng Technol 31(4):325
7. Vinu S (2016) An efficient threshold prediction scheme for wavelet based ECG signal noise reduction using variable step size firefly algorithm. Int J Intell Eng Syst 9(3):117–126
8. Jose J, Gautam N, Tiwari M, Tiwari T, Suresh A, Sundararaj V, Rejeesh MR (2021) An image quality enhancement scheme employing adolescent identity search algorithm in the NSST domain for multimodal medical image fusion. Biomed Signal Process Control 66:102480

9. Haroon M, Gallaghar P, Ahmad M, FitzGerald O (2020) Elevated CRP even at the first visit to a rheumatologist is associated with long-term poor outcomes in patients with psoriatic arthritis. Clin Rheumatol 39:2951–2961
10. Chatterjee S, Dey D, Munshi S (2019) Integration of morphological preprocessing and fractal based feature extraction with recursive feature elimination for skin lesion types classification. Comput Methods Prog Biomed 178:201–218
11. Birkenfeld Judith S, Jason Tucker-Schwartz M, Luis Soenksen R, José Avilés-Izquierdo A, Marti-Fuster B (2020) Computer-aided classification of suspicious pigmented lesions using wide-field images. Comput Methods Prog Biomed 195:105631
12. Zheng Q, Yang M, Yang J, Zhang Q, Zhang X (2018) Improvement of generalization ability of deep CNN via implicit regularization in two-stage training process. IEEE Access 6: 15844–15869
13. Zheng Q, Tian X, Jiang N, Yang M (2019) Layer-wise learning based stochastic gradient descent method for the optimization of deep convolutional neural network. J Intell Fuzzy Syst 37(4): 5641–5654
14. Zheng Q, Tian X, Yang M, Wu Y, Huake S (2019) PACBayesian framework based droppath method for 2D discriminative convolutional network pruning. Multidim Syst Sign Process:1–35
15. Zheng Q, Yang M, Tian X, Jiang N, Wang D (2020) A full stage data augmentation method in deep convolutional neural network for natural image classification. Discret Dyn Nat Soc 2020:1–11
16. Zheng Q, Zhao P, Yang L, Wang H, Yang Y (2020) Spectrum interference-based two-level data augmentation method in deep learning for automatic modulation classification. Neural Comput & Applic:1–23
17. Abbas Z, Rehman MU, Najam S, & Rizvi SD (2019) An efficient gray-level co-occurrence matrix (GLCM) based approach towards classification of skin lesion. In 2019 Amity International Conference on Artificial Intelligence (AICAI) (pp. 317-320). IEEE.
18. Sundararaj V, Selvi M (2021) Opposition grasshopper optimizer based multimedia data distribution using user evaluation strategy. Multimedia Tools and Applications. https://doi.org/10.1007/ s11042-021-11123-4
19. Rejeesh MR, Thejaswini P (2020) MOTF: Multi-objective Optimal Trilateral Filtering based partial moving frame algorithm for image denoising. Multimed Tools Appl 79(37):28411–28430
20. Hassan BA (2021) CSCF: a chaotic sine cosine firefly algorithm for practical application problems. Neural Comput Appl 33(12):7011– 7030
21. Hassan BA, Rashid TA, Mirjalili S (2021) Performance evaluation results of evolutionary clustering algorithm star for clustering heterogeneous datasets. Data in Brief 36:107044
22. Kavitha D, Ravikumar S (2021) IOT and context_ aware learning_ based optimal neural network model for real_ time health monitoring. Trans Emerg Telecommun Tec 32(1):e4132
23. Ravikumar S, Kavitha D (2021) A new adaptive hybrid mutation black widow clustering based data partitioning for big data analysis. Wirel Pers Commun. https://doi.org/10.1007/s11277-021-08516-x
24. Hari V, Neela Madheswari A (2013) Improving security in digital images through watermarking using enhanced histogram modification. In: Meghanathan N, Nagamalai D, Chaki N (eds) Advances in computing and information technology. Advances in Intelligent Systems and Computing, vol 177. Springer, Berlin, Heidelberg. https://doi.org/10.1007/978-3642-31552-7_19
25. Al-Masni MA, Kim DH, Kim TS (2020) Multiple skin lesions diagnostics via integrated deep convolutional networks for segmentation and classification. Comput Methods Prog Biomed 190: 105351
26. Bajwa MN, Muta K, Malik MI, Siddiqui SA, Braun SA, Homey B, Dengel A, Ahmed S (2020) Computer-aided diagnosis of skin diseases using deep neural networks. Appl Sci 10(7):2488
27. Bajwa Usama I, Alam S, Ratyal NI, Anwar MW (2020) Skin disease classification using neural network. Curr Med Imaging 16(6): 711–719
28. Balaji VR, Suganthi ST, Rajadevi R, Krishna Kumar V, Saravana Balaji B, Pandiyan S (2020) Skin disease detection and segmentation using dynamic graph cut algorithm and classification through naive Bayes classifier. Measurement:107922
29. Chatterjee S, Dey D, Munshi S, Gorai S (2019) Extraction of features from cross correlation in space and frequency domains for classification of skin lesions. Biomed Signal Process Control 53: 101581
30. Qin, Zhiwei, Zhao Liu, Ping Zhu, and Yongbo Xue. A GAN-based image synthesis method for skin lesion classification. Computer Methods and Programs in Biomedicine (2020) pp.105568.
31. Zhang X, Wang S, Liu J, Tao C (2018) Towards improving diagnosis of skin diseases by combining deep neural network and human knowledge. BMC medical informatics and decision making 18(2):69–76
32. Khan, Muhammad Attique, Muhammad Younus Javed, Muhammad Sharif, Tanzila Saba, and Amjad Rehman (2019) Multi-model deep neural network based features extraction and optimal selection approach for skin lesion classification. In 2019 international conference on computer and information sciences (ICCIS), pp. 1-7. IEEE.
33. Falcone M, Paolucci G, Tozza S (2020) A high-order scheme for image segmentation via a modified level-set method. SIAM J Imaging Sci 13(1):497–534
34. Vela-Rincón VV, Mújica-Vargas D, Lavalle MM, & Salazar AM (2020) Spatial $$\alpha $$-trimmed fuzzy c-means algorithm to image segmentation. In Mexican Conference on Pattern Recognition (pp. 118-128). Springer, Cham.

35. Selvi Thamil J (2020) Segmentation and validation of infrared breast images using weighted level set and phase congruency edge map framework. Signal and Image Processing Techniques for the Development of Intelligent Healthcare Systems. Springer, Singapore pp. 87-102.
36. Dijk V, Nico P, Maute K, Langelaar M, Van Keulen F (2013) Level-set methods for structural topology optimization: a review. Struct Multidiscip Optim 48(3):437–472
37. Li BN, Chui CK, Chang S, Ong SH (2011) Integrating spatial fuzzy clustering with level set methods for automated medical image segmentation. Comput Biol Med 41(1):1–10
38. Yushkevich Paul A, Piven J, Hazlett HC, Smith RG, Ho S, Gee JC, Gerig G (2006) Userguided 3D active contour segmentation of anatomical structures: significantly improved efficiency and reliability. Neuroimage 31(3):1116–1128
39. Cheng Y, Swamisai R, Umbaugh SE, Moss RH, Stoecker WV, Teegala S, Srinivasan SK (2008) Skin lesion classification using relative color features. Skin Res Technol 14(1):53–64
40. Moreno PJ, Ho PP, & Vasconcelos N (2004) A Kullback-Leibler divergence based kernel for SVM classification in multimedia applications. In Advances in neural information processing systems (pp. 1385-1392).
41. Hayyolalam V, Kazem AAP (2020) Black widow optimization algorithm: a novel metaheuristic approach for solving engineering optimization problems. Eng Appl Artif Intell 87:103249
42. Korovkinas, Konstantinas, Paulius Danenas, and G. Garšva. Support vector machine parameter tuning based on particle swarm optimization metaheuristic. Nonlinear Analysis: Modelling and Control 25(2) (2020) 266-281.
43. Manerkar Mugdha S, Snekhalatha U, Shashwata Harsh, Juhi Saxena, Simanta Sarma P, and Anburajan M (2016) Automated skin disease segmentation and classification using multi-class SVM classifier
44. Codella Noel, Veronica Rotemberg, Philipp Tschandl, Emre Celebi M, Stephen Dusza, David Gutman, Brian Helba et al. (2019) Skin lesion analysis toward melanoma detection 2018: a challenge hosted by the international skin imaging collaboration (isic). arXiv preprint arXiv:1902.03368